

27. Hoare, J. P., *Nature* (1968) **219**, Sept. 7, 1034.
28. Chin, D. T., in *Fundamentals of Electrochemical Machining* (see Ref. 8), p. 250.
29. Mao, K. W., Hoare, J. P. and Wallace, A. J., *J. Electrochem. Soc.* (1972) **119**, No. 4, 419.
30. Chin, D. T., *J. Electrochem. Soc.* (1972) **119**, No. 8, 1043.
31. Boden, P. J. and Evans, J. M., *Nature* (1969) **222**, 337.
32. Boden, P. J. and Evans, J. M., *Electrochim. Acta* (1971) **16**, 1071.
33. LaBoda, M. A., Chartrand, A. J., Hoare, J. P., Wiese, C. R. and Mao, K. W., *J. Electrochem. Soc.* (1973) **120**, No. 5, 646.
34. Evans, J. M. and Boden, P. J. in *Fundamentals of Electrochemical Machining* (see Ref. 8), p. 40.
35. Fitz-Gerald, J. M. and McGeough, J. A., Paper presented at I.E.E. Conf. on Electrical Methods of Machining, Forming and Coating, London. Conf. Public. No. 61 (1970) p. 72.
36. Hopenfeld, J. and Cole, R. R., *Trans. A.S.M.E. Series B, J. Eng. Ind.* (1969) Aug., 755.
37. De la Rue, R. E. and Tobias, C. W., *J. Electrochem. Soc.* (1959) Sept., 827.
38. Wagner, C., in *Advances in Electrochemistry and Electro-Chemical Engineering* (ed. P. Delahay and C. W. Tobias), Interscience (1962) **2**, 1.
39. Cook, N. H., Loutrel, S. P. and Meslink, M. C., *Increasing ECM Rates*, Mass. Inst. of Tech. Report (1967).
40. Lovering, D. G., Paper presented at 23rd Meeting, I.S.E., Stockholm, Aug.-Sept. 1972.
41. Gurkis, J. A., *Metal Removal by Electrochemical Methods and Its Effect on Mechanical Properties of Metals*, Defence Metals Information Center, Report 213, Battelle Memorial Institute (1965) Jan.
42. Evans, J. M., Boden, P. J. and Baker, A. A., Proc. 12th Int. Mach. Tool Des. Res. Conf., Macmillan (1971) p. 271.
43. Zimmel, L. J., Paper presented at U.S. Nat. Aero- and Space Eng. Meeting, Oct. 1964.
44. Bannard, J., Paper presented at First Int. Conf. on ECM, Leicester Univ., Mar. 1973.
45. Bayer, J., Cummings, M. A. and Jollis, A. U., Gen. Electric Co., Final Report on Electrolytic Machining Development, Rep. No. ML-TDR-64-313 (1964) Sept.

## CHAPTER FIVE

**Dynamics and Kinematics**

Studies of the behaviour of metal-electrolyte combinations for the conditions of ECM must eventually be utilised in applications of the process. In these applications, certain dynamical and kinematic features of the process are invariably exhibited. If one electrode, the cathode, say, is fed towards the other, the width of the gap between the electrodes will eventually become steady.\* This equilibrium gap is a consequence of an inherent feature of ECM whereby the rate of forward movement of the cathode becomes matched by the local

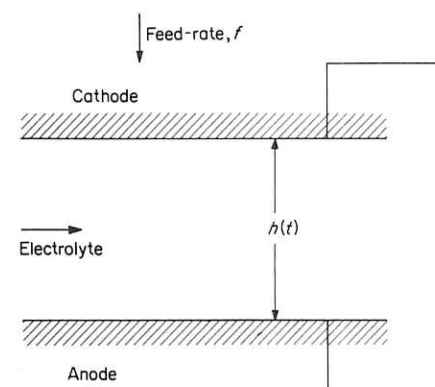


Fig. 5.1 Set of plane parallel electrodes

\* The inter-electrode gap referred to here and elsewhere in the text is occasionally referred to as the 'end gap'. Cases in which some other gap is considered should be clear from the discussion at the appropriate part of the text.

anodic dissolution rate. If the cathode is not so moved, the gap will increase indefinitely as machining proceeds.

But these trends of behaviour are subject to other influences. Cathodic gas generation and electrical heating, due to the passage of current, can cause the width of the equilibrium gap to become tapered along the length of the electrode. These two processes have diverse other effects in ECM. Moreover, if they are not controlled, they can lead to the premature termination of machining, although this condition can also be produced by other electrochemical and hydrodynamic factors.

### 5.1 Variation of gap width with machining time

#### 5.1.1 Direct current

Consider a set of plane parallel electrodes with a constant potential difference  $V$  applied across them and with the cathode moving towards the anode at a constant rate  $f$ . The electrode configuration is shown in Fig. 5.1. The electrolyte is assumed to be flowing at such a rate that its conductivity in the gap remains constant. For the present, the effect of overpotentials will not be considered, and field effects at the edges of the electrode are ignored. Under these conditions, the width of the gap between the electrodes can be taken to be dependent only on machining time. Let the gap at the start of machining be  $h(0)$ , and after time  $t$  let it be  $h(t)$ . If 100% current efficiency is also assumed, then from Faraday's law, the rate of change of gap relative to the cathode surface is

$$\frac{dh}{dt} = \frac{AJ}{z\rho_a F} - f \quad (5.1)$$

where, as defined previously,  $A$ ,  $z$ , and  $\rho_a$  are the atomic weight, valency, and density of the anode metal,  $J$  is the current density, and  $F$  is Faraday's constant.

For a constant electrolyte conductivity, Ohm's law gives

$$J = \frac{\kappa_e V}{h} \quad (5.2)$$

On substitution into Equation (5.1):

$$\frac{dh}{dt} = \frac{MV}{h} - f \quad (5.3)$$

where  $M (= A\kappa_e/zF\rho_a)$  is a machining parameter.

Equation (5.3) has the solution

$$t = \frac{1}{f} \left[ h(0) - h(t) + h_e \ln \frac{h(0) - h_e}{h(t) - h_e} \right] \quad (5.4)$$

where

$$h_e = \frac{MV}{f} \quad (5.5)$$

is the equilibrium gap, the steady-state solution to Equation (5.3) for  $dh/dt = 0$ . A useful relationship for determining equilibrium feed-rates can also be obtained from Equations (5.2) and (5.5):

$$f = \frac{e_a J}{\rho_a} \quad (5.6)$$

where  $e_a (= A/zF)$  is the electrochemical equivalent for the anode metal.

Three practical cases are now of interest:

- (a) When  $f = 0$ , that is, no cathode movement, Equation (5.3) has the solution

$$h^2(t) = h^2(0) + 2Mvt \quad (5.7)$$

The gap then increases indefinitely with the square root of the machining time (Fig. 5.2).

- (b) An ever increasing gap is not usually desirable in ECM, particularly when an accurate shape has to be produced on the anode. Accordingly, fixed mechanical movement of the cathode is much more common. Thus, when Equation (5.4) is used to compare the gap

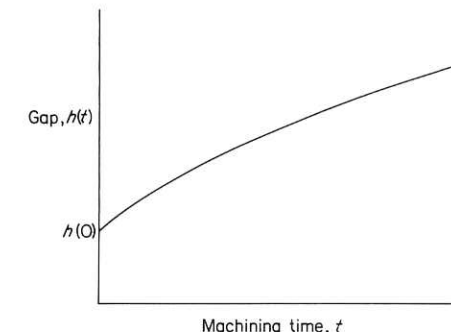


Fig. 5.2 Indefinite increase of gap with machining time (zero feed-rate)

width with machining time, and if the initial gap is greater than the final gap, the gap width is seen to decrease with time to its equilibrium value. When the gap is initially smaller than the steady-state value, it

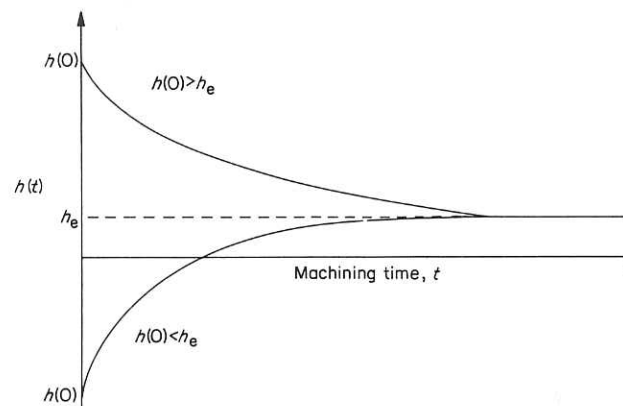


Fig. 5.3 Variation of gap width with machining time (constant feed-rate)

increases to the equilibrium width. This dependence of gap width on machining time is illustrated in Fig. 5.3.

(c) Finally, the condition  $h(t) = 0$  implies a short circuit between the electrodes; and values of  $h(t)$  less than zero are physically impossible.

#### Example

For typical values,  $e_a = 29 \times 10^{-5}$  g/C,  $\kappa_e = 0.2 \text{ ohm}^{-1} \text{ cm}^{-1}$ ,  $\rho_a = 8 \text{ g/cm}^3$ ,  $V = 10 \text{ V}$ , and  $f = 1.66 \times 10^{-2} \text{ mm/s}$ , we obtain from Equation (5.5) that  $h_e = 0.44 \text{ mm}$ .

In Equation (5.6), suppose that  $J = 50 \text{ A/cm}^2$ , with the same values for  $e_a$  and  $\rho_a$  as above. Then  $f$  is calculated to be  $1.8 \times 10^{-2} \text{ mm/s}$ .

The above analyses have been carried out without the complications of overpotentials at the electrodes. In Chapter 3 it was proposed that for ECM conditions the concentration overpotential may be considered to be negligible and that a Tafel expression may be used for the activation overpotential. In the Tafel equation, this overpotential varies only slowly with current density, and in most ECM analyses it is considered constant. Equation (5.5) may then be modified to account for overpotentials:

$$h_e = \frac{M(V - \Delta V)}{f} \quad (5.8)$$

where  $\Delta V$  describes the sum of the electrode overpotentials, including reversible potentials, and it is assumed to have a constant value.

#### Example

Suppose that the sum of the overpotentials and reversible potentials comes to 2 V. From Equation (5.8), the corresponding value for  $h_e$  is found to be 0.35 mm, the same values being retained for the other process variables used in the previous example.

Finally, a non-dimensionalised treatment of these basic equations is of interest here, in which a non-dimensional function  $\psi$  has been defined:

$$\psi = \left[ \frac{fh(0)}{A\kappa_e(V - \Delta V)} \right] \frac{zF\rho_a}{zF\rho_a} \quad (5.9)$$

This function includes all the dynamic and electrochemical features of the process for the conditions stated above. For the cases  $\psi < 1$  and  $\psi > 1$ , the gap width respectively increases and decreases with machining time to the equilibrium gap width, and for  $\psi = 1$ , the gap width always has its equilibrium value [1].

#### 5.1.2 A practical case

The practice of electrochemical deep-hole drilling is a case where part of an anode surface can be machined under conditions of a

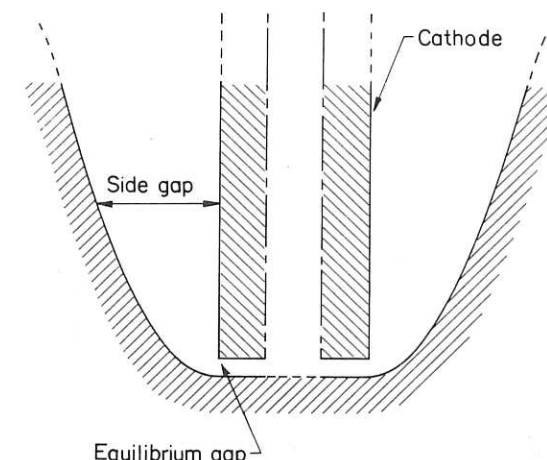


Fig. 5.4 Electrochemical drilling; forward gap (equilibrium) and side gap

constant cathode feed-rate, whilst another part is subject to conditions of zero effective feed-rate. Figure 5.4 illustrates such a case for a cylindrical cathode moving into an anode, the direction of the cathode feed-rate being along the axis of the cathode.

Suppose, first, that machining only takes place over that region of the anode directly adjacent to the leading edge of the cathode. Since ECM there is in the direction of cathode feed, an equilibrium gap will be obtained under the conditions specified by Equation (5.5).

Next, consider dissolution only in the radial direction from the cathode, with ECM in the region of its leading edge ignored. The effective feed-rate normal to the cathode surface is zero, and under that condition, dissolution of the side walls of the anode takes place. The local difference between (i) the radial length between the side wall of the anode and the central axis of the cathode, and (ii) the external radius of the cathode is known as the overcut. The amount of overcut can be diminished by several devices, including insulation along the external side walls of the cathode, so that closer accuracy of machining can be maintained. The relationship between the overcut and the equilibrium gap at the leading edge, for both insulated and non-insulated cathode side walls, is discussed in Chapter 7. (It should be remembered that other effects, e.g. those due to electrolyte flow and gas generation, have been omitted in this brief presentation of drilling.)

### 5.1.3 Alternating current

Although direct current (d.c.) is, by far, more common in ECM, its replacement by alternating current (a.c.) has received some attention [2-4]. The apparent advantage of the use of the latter type of supply is that the need for rectification of the very high currents is abolished. However, on economic grounds, the practical use of a.c. appears to require two further conditions. First, cathode materials such as titanium diboride have to be used, which rectify, at least in part, the current in the electrolytic cell. Secondly, some form of twin cell machining is essential so that alternate dissolution of two anodes can take place.

In this section, the discussion of alternating current is restricted to a simple analysis of the dependence of gap width on machining time. With reference to Fig. 5.1, the constant potential difference  $V$  is now assumed to be replaced by an applied voltage, of sinusoidal waveform and of r.m.s. value  $V_{\text{rms}}$ . The cathode material is considered to be inert; it is not dissolved during the reverse part of the current

cycle for which it is anodic. The other assumptions made above are retained with one main exception. Since machining can only take place during one half of each time cycle, the maximum current efficiency can only approach 50%. Experiments have shown that the efficiency is often considerably less, and values about 20 to 30% are common.

For the portion of the time cycle during which the true anode is machined, the rate of change of gap width relative to the cathode surface is given, from Faraday's law, as

$$\frac{dh}{dt} = \frac{e_a J \Gamma}{\rho_a} - f \quad (5.10)$$

where  $\Gamma$  is the current efficiency.

The effective applied voltage  $V$  can be expressed in terms of  $V_{\text{rms}}$ :

$$V = (\sqrt{2} V_{\text{rms}} - \Delta V) \sin \omega t \quad (5.11)$$

where  $\Delta V$  is an expression, assumed constant, for the sum of the reversible potentials and overpotentials at the electrodes.

By use of Ohm's law, Equation (5.10) becomes

$$\frac{dh}{dt} = \frac{(\sqrt{2} V_{\text{rms}} - \Delta V) e_a \kappa_e \Gamma \sin \omega t}{h \rho_a} - f \quad (5.12)$$

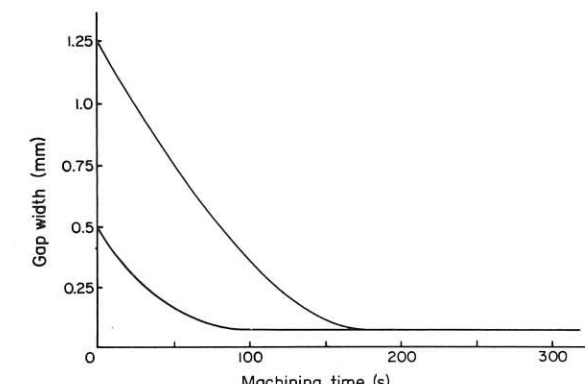


Fig. 5.5 Variation of gap width with machining time (alternating current);  $e_a = 25 \times 10^{-5} \text{ g/C}$ ;  $\Gamma = 0.26$ ;  $\rho_a = 7.7 \text{ g/cm}^3$ ;  $\kappa_e = 0.195 \text{ ohm}^{-1} \text{ cm}^{-1}$ ;  $V_{\text{rms}} = 12 \text{ V}$ ;  $\Delta V = 1.4 \text{ V}$ ;  $f = 10^{-2} \text{ mm/s}$ ;  $h(0) = 1.25, 0.5 \text{ mm}$

During the other part of the time cycle for which the true cathode becomes the positive electrode,

$$\frac{dh}{dt} = -f \quad (5.13)$$

These equations can be solved numerically to give the gap as a function of time. The results for typical values given in Fig. 5.5 demonstrate that a steady-state gap is achieved in a.c. ECM. The existence of equilibrium gap conditions in a.c. ECM has been confirmed experimentally [2], the above theory being shown to provide a reasonable description of a.c. ECM, despite the number of simplifying assumptions.

## 5.2 Hydrogen evolution

So far, the influence of the other processes at work in ECM has not been considered. For example, the usual complementary reaction at the cathode, hydrogen evolution, usually reduces the effective conductivity of the electrolyte so that the local anodic dissolution rate varies downstream until equilibrium is achieved. We have seen earlier that the passage of current increases the conductivity by Joule heating, so lessening the effect due to hydrogen. The effects of

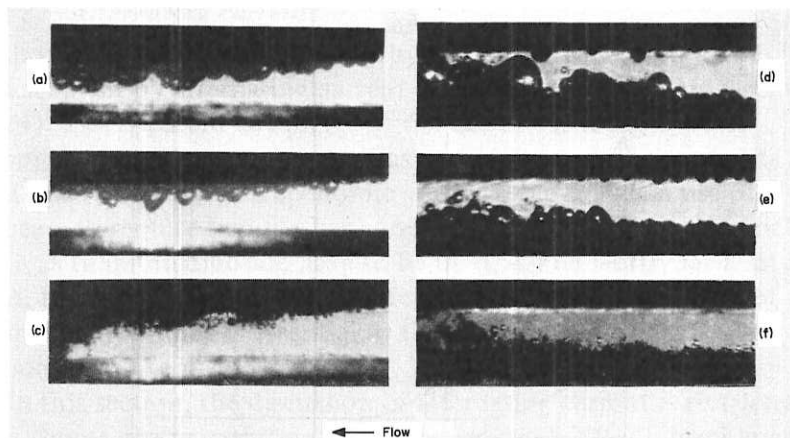


Fig. 5.6 Effect of electrolyte flow velocity and cathode orientation on gas generation in 2N KCl; current density 50 A/cm<sup>2</sup>, electrode gap 0.5 mm. Cathode face down: flow velocity (a) 1 m/s, (b) 2 m/s, (c) 4 m/s. Cathode face up: flow velocity (d) 1 m/s, (e) 2 m/s, (f) 4 m/s. (By permission of Landolt, Acosta, Muller and Tobias [5])

these processes can be analysed from a study of the transport processes appropriate to ECM. It should help in these studies to have some appreciation of (i) the location of bubbles in the machining gap, and (ii) the effects on the size and location of the bubbles of process variables. To this end, some photographic investigations are of interest [5-9].

The formation next to the cathode surface of the hydrogen gas bubble layer can be seen from photographs of the electrode gap region (Fig. 5.6); the related experimental data are also given. The thickness of the bubble layer increases in the downstream direction along the gap, and it decreases as the electrolyte flow-rate is increased. Further photographs demonstrate that the size of individual bubbles also decreases rapidly as the electrolyte velocity is increased from

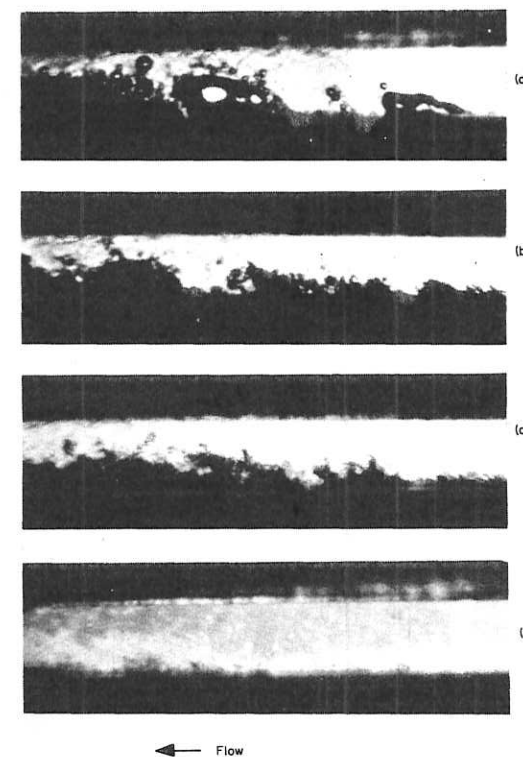


Fig. 5.7 Effect of flow velocity on hydrogen gas evolution in 2N KCl; current density 100 A/cm<sup>2</sup>. Cathode face up: flow velocity (a) 4 m/s, (b) 6 m/s, (c) 10 m/s, (d) 25 m/s. (By permission of Landolt, Acosta, Muller, and Tobias [5])

4 to 25 m/s (current density,  $100 \text{ A/cm}^2$ ) (Fig. 5.7). From Fig. 5.8, the bubble size is seen to increase with increasing current density, the flow-rate being held constant.

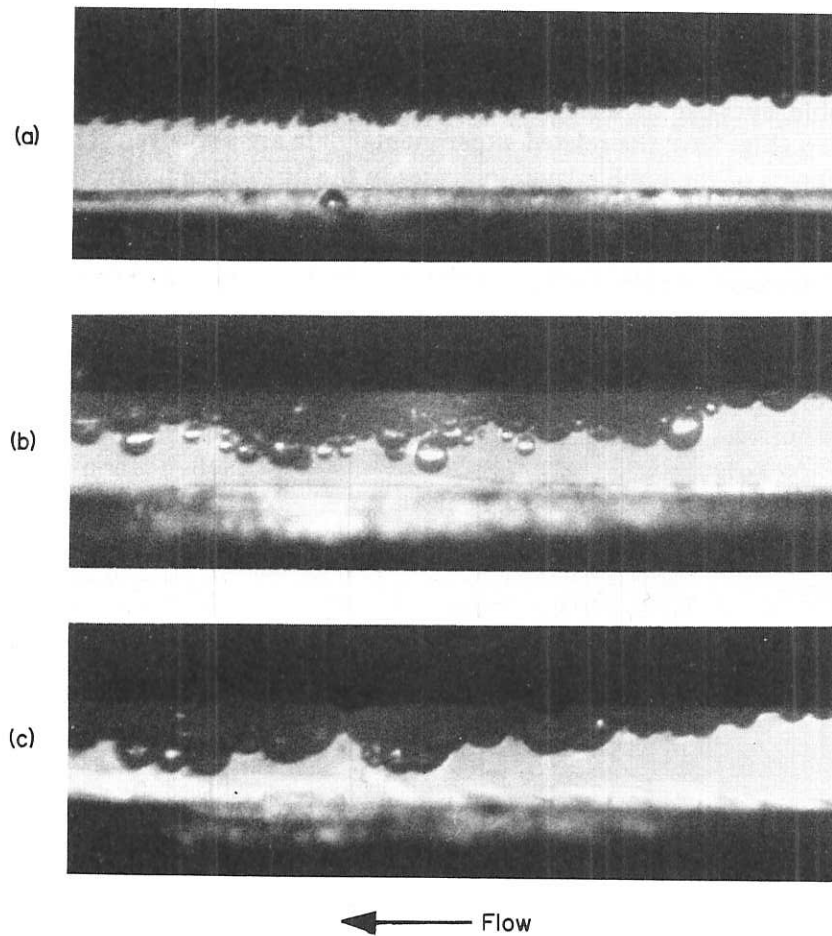


Fig. 5.8 Effect of current density on cathodic gas generation in 2N KCl. Cathode face down. Electrolyte velocity 1 m/s; current density (a)  $5 \text{ A/cm}^2$ , (b)  $20 \text{ A/cm}^2$ , (c)  $50 \text{ A/cm}^2$  (By permission of Landolt, Acosta, Muller, and Tobias [5])

These observations show that the gas bubbles occupy a region adjacent to the cathode, and that they are not dispersed uniformly throughout the machining gap. From Fig. 5.6, the thickness of the

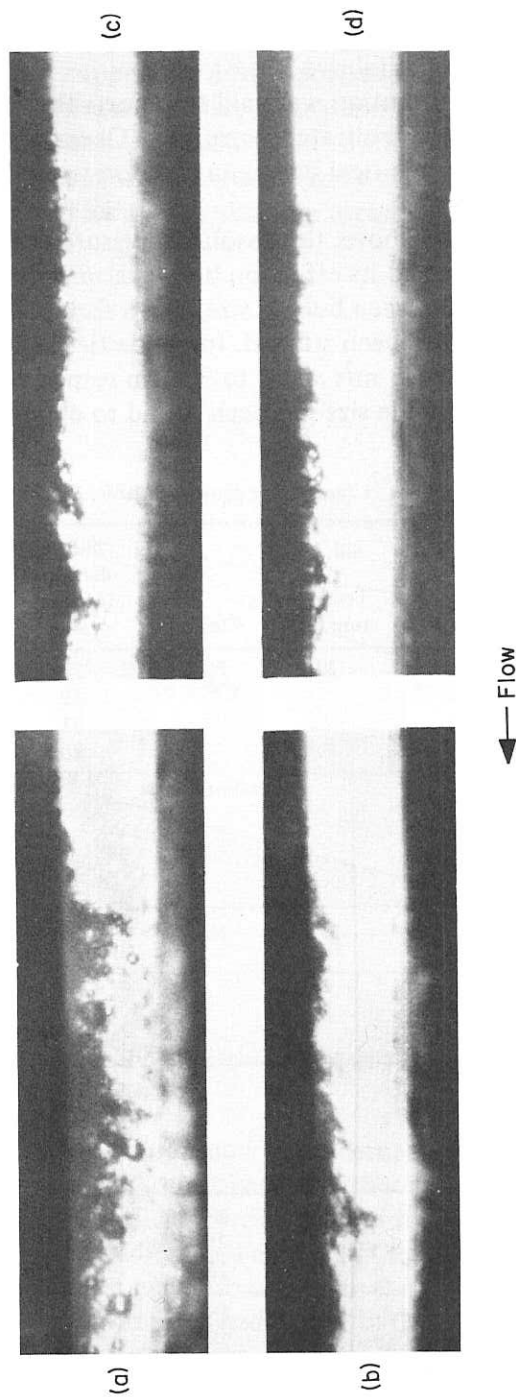


Fig. 5.9 Cathodic gas generation in 2N  $\text{KNO}_3$  and 2N KCl. Current density  $100 \text{ A/cm}^2$ . Cathode face down. Electrolyte velocity (KCl) (a) 4 m/s, (b) 8 m/s; (KNO<sub>3</sub>) (c) 4 m/s, (d) 8 m/s (By permission of Landolt, Acosta, Muller, and Tobias [5])

two-phase region is noted to be independent of orientation of the cathode for high velocities (above 1 m/s).

In Chapter 4, some attention was paid to reports that very little cathodic gas is produced in nitrate electrolytes. Observational proof is given in Fig. 5.9, for identical machining conditions in chloride and nitrate electrolytes.

In the work described above, the absolute pressure at the electrodes was about atmospheric and its effect on bubble size was negligible [5]. The relationship between bubble size, mean flow velocity, and absolute pressure has also been studied, for velocities and pressures ranging from about 4 to 18 m/s and 2 to 30 atm respectively [8, 9]. From this study, the bubble size has been found to decrease also

Table 5.1 Mean bubble diameter as a function of process variables

Current density (A/cm <sup>2</sup> )	Electrolyte velocity (m/s)	Absolute pressure (approx) (atm)	Temperature (°C)	Electrolyte	Bubble diameter (approx) (μm)	Other information	Ref.
4.7	32	27	NaCl	50	Mild steel	9	
	16			62			
	8			81	anode, brass		
	6			90	cathode, no hydrodynamic entry length		
	2.5			130			
10.8	32	27	NaCl	35		9	
	16			45			
	8			55			
	6			62			
	2.5			75			
18	16			27		9	
	6			33			
	4			40			
	2.5			47			
50	1	1-1.3	25	2N KCl	99	copper electrodes	5
50	2	1-1.3	25	2N KCl	69		
50	4	1-1.3	25	2N KCl	35		
5	1	1-1.3	25	2N KCl	56	copper electrodes	5
20	1	1-1.3	25	2N KCl	78		
50	1	1-1.3	25	2N KCl	99		

with increasing pressure and velocity; for any given velocity, the bubble diameter appears to be proportional to  $(\text{pressure})^{-0.3}$

Table 5.1 carries a summary of experimental data on bubble size for ECM conditions. The table again confirms that bubble size increases with increasing current density and decreases with increasing electrolyte velocity and absolute pressure.

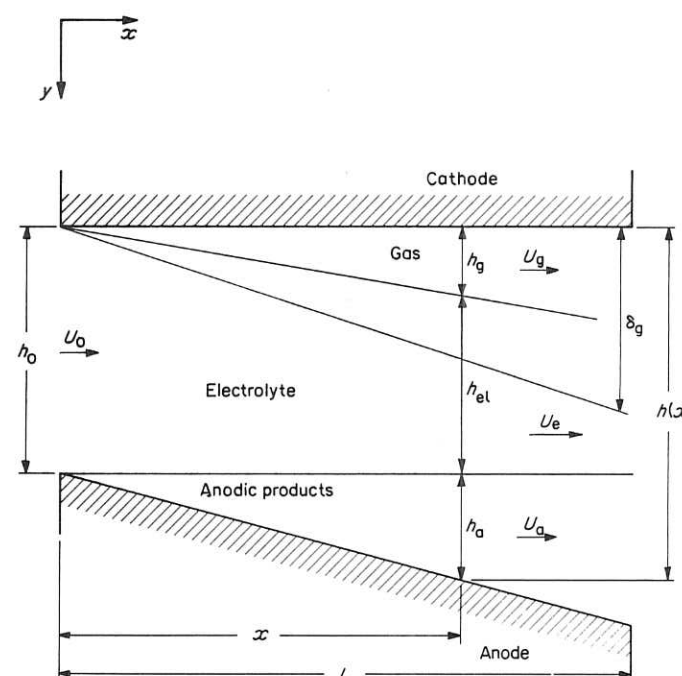


Fig. 5.10 Variation in gap width (after Thorpe and Zerkle [10])

Although the discussion now is concerned with gas evolved at the cathode, it is relevant to recollect here that gas can be evolved at the anode. Current efficiency calculations for gas generation at both electrodes have been discussed earlier in Chapter 4. It should be recalled that bubbles may also appear in the gap due to cavitation. This phenomenon was discussed earlier in Chapter 2. In subsequent sections of the present chapter, only hydrogen gas evolution at the cathode is considered, and 100% efficiency is assumed.

### 5.3 Transport equations

The principal processes at work in ECM were discussed in Chapters 1 to 3, and many aspects of their bearing on the rate and manner of the electrode reactions were brought to light in Chapter 4.

There are, of course, many other effects, and some are now studied which influence the dynamic and kinematic behaviour of the process. In particular, we shall examine some effects due to hydrogen gas evolution and electrical heating. Initially, the discussion will be restricted to modifications which they impose on the shape of the equilibrium gap. That the effective conductivity of the electrolyte solution is changed sufficiently by gas and heating to produce a tapering of an otherwise parallel gap is often a major problem in cathode design.

This problem can be tackled with the aid of the appropriate transport equations of mass, energy, and electrical charge in ECM, several simplified models of which are available [7, 10–12]. Of these models, one yields essentially a computer solution of the transport equations [7], whilst the others supply an analytic solution. We follow the latter argument, keeping in mind that the model incorporates some assumptions which may not necessarily apply in practice and that it omits some physical features of ECM. Nevertheless, much useful information can still be deduced from it.

#### 5.3.1 Introductory equations

Figure 5.10 accounts for the modified shape of the equilibrium gap. Since steady-state machining conditions are assumed, the gap does not change further with machining time. But its equilibrium width does now vary with distance  $x$  along the electrode length. As only equilibrium conditions are considered, we can also drop the subscript e without loss of meaning; the gap now varies from its width at inlet,  $h_0$ , in some undefined fashion to its value  $h(x)$  downstream. The cathode still moves towards the anode at a fixed rate  $f$ . The electrolyte velocity is assumed to have values  $U_0$  at inlet and  $U(x)$  downstream; the velocity is also assumed to have no variation in the  $y$  direction.\* The current density  $J$  causes hydrogen gas to be evolved in the vicinity of the cathode at a local flux rate  $m_g$  (mass

\* Since the electrolyte velocity is assumed to have no variation across the electrode gap width, the symbol  $U$  is now used for the velocity, in common with the usual notation for ECM.

per unit time per unit area). The hydrogen gas is considered to flow at some rate which is equivalent to the local layer width  $h_g$ , the gas bubbles being contained within an electrolyte layer of thickness  $\delta_g$ . If the bubbles occupy the whole channel, then  $\delta_g = h$ . This condition may arise at some distance downstream. If the bubbles become completely coalesced, then  $\delta_g = h_g$ , and they would then be completely separated from the pure electrolyte. (ECM would also be terminated because the cathode would be insulated from the anode.) The anodic reactions result in an equivalent layer (for example, of metal hydroxide) at the anode of local width  $h_a$ , the local flux rate being  $m_a$ . The central region, of width  $h_{el}$  is occupied by pure electrolyte.\* The three phases, gas, anodic products, and electrolyte, are assumed to flow in the downstream direction with a local average velocity in some area proportional to the width  $h$ . That is,

$$\begin{aligned} U_g &\propto h_g \\ U_e &\propto h_{el} \\ U_a &\propto h_a \end{aligned} \quad (5.14)$$

Also,

$$h(x) = h_g + h_{el} + h_a \quad (5.15)$$

The gas phase fraction,  $\alpha$ , and anodic products fraction,  $\beta$ , can now be conveniently defined as

$$\begin{aligned} \alpha &= \frac{h_g}{h} \\ \beta &= \frac{h_a}{h} \end{aligned} \quad (5.16)$$

The equivalent relationship for the electrolyte then is

$$(1 - \alpha - \beta) = \frac{h_{el}}{h} \quad (5.17)$$

\* To avoid confusion with the recognised symbol for the equilibrium gap,  $h_e$ , the subscript 'el' is used here to identify the thickness of the layer of pure electrolyte. The subscript 'e' is retained to denote the other properties of the pure electrolyte layer.

Corresponding fractions for the mass flow-rates of hydrogen gas and anodic products can be expressed in terms of the individual mass flow-rates:

$$\mu = \frac{\omega_g}{\omega}$$

$$\nu = \frac{\omega_a}{\omega} \quad (5.18)$$

$$(1 - \mu - \nu) = \frac{\omega_e}{\omega}$$

where

$$\omega = \omega_g + \omega_e + \omega_a \quad (5.19)$$

$$\omega_g = \rho_g h_g U_g$$

Similar expressions apply for  $\omega_a$  and  $\omega_e$ .

The slip ratios  $\sigma$  and  $\Omega$  are defined by

$$\sigma = \frac{U_g}{U_e}$$

$$\Omega = \frac{U_a}{U_e} \quad (5.20)$$

Certain approximations, which are valid in practice, can ease the subsequent analysis. In Chapter 4, it was stated that the anodic products in solution have negligible effect on the density and conductivity of the bulk solution. Moreover, Thorpe and Zerkle have proposed that, for inlet electrolyte pressures of the order of 690 kN/m<sup>2</sup> (which are typical for ECM),  $\beta$  is much smaller than  $\alpha$ . It is reasonable then to assume that  $h_a$ ,  $U_a$ , and  $\beta$  are negligible.

Before we proceed further, it may be helpful to identify more fully the notion of the mass flux rate  $m_a$ . From Faraday's law,

$$m_a = e_a J \quad (5.21)$$

Since, for equilibrium ECM,

$$J = \frac{\rho_a f}{e_a} \quad (5.6)$$

we have

$$m_a = \rho_a f \quad (5.22)$$

which is a measure of the local rate of recession of the anode surface in the direction normal to the cathode surface.

### 5.3.2 Equation of continuity of mass

A volume control element in the inter-electrode gap is shown in Fig. 5.11. Since the anodic products are considered to have negligible effect, only the hydrogen gas and pure electrolyte phases are shown.

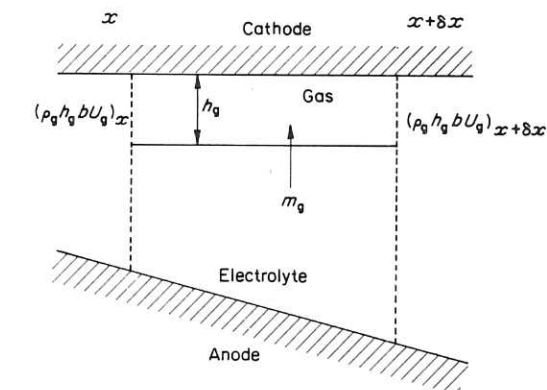


Fig. 5.11 Control volume element for continuity of mass

They are assumed to occupy the regions indicated. For the purposes of the analysis, the hydrogen gas is assumed to be evolved at the interface between the electrolyte and gas phases, and to enter the gas control element. If the principle of conservation of mass for flow in a duct is applied, analysis yields the equation of continuity of mass flow from section to section.

Applying the law of conservation of mass to the gas-phase control volume, we see that

$$(\rho_g h_g b U_g)_x + m_g \delta x b = (\rho_g h_g b U_g)_{x+\delta x} \quad (5.23)$$

where  $b$  is the electrode width. In the limit  $\delta x \rightarrow 0$ , this becomes

$$\frac{d}{dx} (\rho_g h_g U_g) = m_g \quad (5.24)$$

From Equations (5.16) and (5.20), and since

$$m_g = e_g J$$

we obtain

$$\frac{d}{dx}(\rho_g \alpha \sigma h U_e) = e_g J \quad (5.25)$$

A similar equation can be derived for the electrolyte component:

$$\frac{d}{dx}[\rho_e(1 - \alpha)hU_e] = (e_a - e_g)J \quad (5.26)$$

### 5.3.3 Energy equation

Consider the volume element for energy balance shown in Fig. 5.12. Hopfenfeld and Cole [7] have enumerated the relevant factors which contribute to generation of heat within the volume element: (a) Joule heating, (b) irreversible energy released from electrochemical reactions at the surfaces of the electrodes, (c) energy due to secondary chemical reactions in the bulk of the electrolyte, (d) the reversible heat of the electrochemical reactions, (e) heat lost or added to the fluid from the surrounding surfaces, e.g. the walls of the electrodes, and (f) the mechanical heat generated in the fluid by the viscous component of the flow. Any subsequent analysis can be considerably simplified if the reasonable assumption is made that the heat arising from the contributions (b) to (f) is negligible compared with that from (a). If the heat capacity and thermal conductivity of the gas phase are also assumed to be sufficiently low, the hydrogen can be assumed to absorb none of the electrical energy

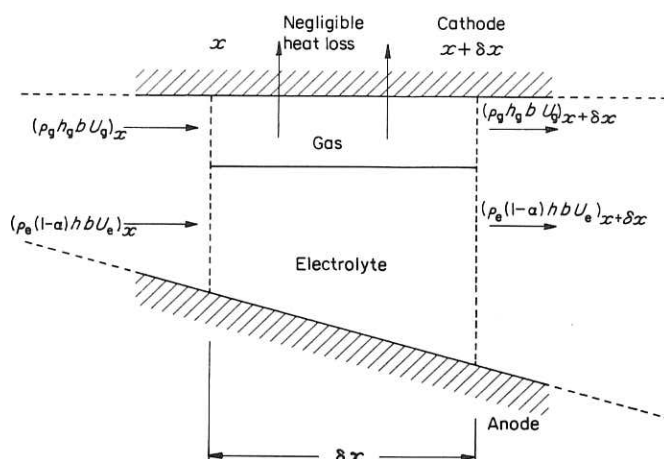


Fig. 5.12 Control volume element for continuity of energy

dissipated between the electrodes. Then only the liquid electrolyte phase has to be considered.

Assuming now that the electrical energy added to the volume element is dissipated as heat in the electrolyte, we deduce the temperature gradient,

$$\frac{dT}{dx} = \frac{J(V - \Delta V)}{c_e(1 - \alpha)h\rho_e U_e} \quad (5.27)$$

where  $c_e$  is the specific heat of the electrolyte.

Thorpe and Zerkle also give the equations of state for the gas and electrolyte as

$$\rho_g = \frac{p}{RT} \quad (5.28)$$

$$\rho_e = \rho_0 \quad (5.29)$$

where  $p$  is the static pressure,  $R$  is the Gas Constant, and  $T$  is the temperature. The suffices  $g$  and  $e$  denote the quantity for the gas and electrolyte whilst the suffix 0 denotes inlet conditions.

### 5.3.4 Equation for balance of electrical charge

For the electrical charge across the volume element to be balanced, its distribution at the metal-electrolyte interfaces, across the diffusion layers, and at the outer boundaries of the diffusion layers must be known, as well as the particular electrochemical reaction. This information is difficult to find. Indeed, Bass [13] has pointed out the difficulties of balancing the charge just within the diffusion layer with the charge in the region just outside it. A commonly accepted, simpler approach is to use a form of Ohm's law to describe the balance of charge across the gap:

$$J = \frac{\kappa_m(V - \Delta V)}{h} \quad (5.30)$$

where  $\kappa_m$  is the conductivity of the electrolyte-gas medium. Next, as proposed by Thorpe and Zerkle, the gas-phase fraction is regarded as equivalent to the void fraction. Then, from the work of De la Rue and Tobias [14], the conductivity  $\kappa_m$  can be expressed further in terms of the electrolyte conductivity,  $\kappa_e$ , and the void fraction,  $\alpha$ , by use of the Bruggeman equation:

$$\kappa_m = \kappa_e(1 - \alpha)^n \quad (5.31)$$

The power  $n$  is normally 1.5. For  $\alpha$  sufficiently small, say  $\alpha < 0.2$ , this equation can be approximated by

$$\kappa_m = \kappa_e(1 - 1.5\alpha) \quad (5.32)$$

An expression can also be obtained from Ohm's law which relates  $\kappa_m$  and  $\kappa_e$  with the thickness  $\delta_g$  of the layer containing the hydrogen bubbles:

$$(V - \Delta V) = \frac{J\delta_g}{\kappa_m} + \frac{J(h - \delta_g)}{\kappa_e} \quad (5.33)$$

Here it is assumed that  $\delta_g = h$  at outlet.

It has been pointed out earlier that the conductivity  $\kappa_e$  also depends on temperature:

$$\kappa_e = \kappa_0[1 + \zeta(T(x) - T_0)] \quad (5.34)$$

where  $\kappa_0$  is the conductivity of the electrolyte at inlet,  $\zeta$  is the temperature coefficient for conductivity,  $T(x)$  is the temperature at some control point, and  $T_0$  is the temperature at inlet.

### 5.3.5 Discussion of quasi-steady processes

The stage has now almost been reached where the transport equations can be used to investigate the modifications imposed on the shape of the equilibrium gap by the gas and electrical heating. Before this can be done, however, one other matter needs consideration. The void fraction, the solution temperature, and the velocity themselves have a response to the changes in the gap conditions caused by the gas and heating. We must, therefore, examine the time taken for the void fraction, the solution temperature, and velocity within the gap to reach an equilibrium state.

In the study of this problem, it is convenient to write the governing kinematic equation (5.3) in the form

$$\frac{1}{f} \frac{\partial h}{\partial t} = \frac{J(t)}{J} - 1$$

where for clarity the symbol  $J(t)$  is now a time-dependent current density whilst the symbol  $J$  is retained for the equilibrium current density:

$$J = \lim_{t \rightarrow \infty} J(t) = \frac{f\rho_a}{e_a}$$

Previously, the void fraction and slip ratio have been defined by

$$\alpha = \frac{h_g}{h} \quad \text{and} \quad \sigma = \frac{U_g}{U_e}$$

Next, a set of characteristic dimensionless variables are introduced which have unit order of magnitude at some location along the gap:

$$\begin{aligned} x^0 &= \frac{x}{L}, & t^0 &= \frac{ft}{h_0} \\ h^0 &= \frac{h}{h_0}, & U^0 &= \frac{U}{U_0} \\ T^0 &= \frac{T}{T_0}, & \rho^0 &= \frac{\rho}{\rho_0}, & p^0 &= \frac{p}{p_0} \end{aligned} \quad (5.35)$$

Now consider the equation of continuity of mass. It can be readily deduced that its time-dependent form is

$$\frac{\partial}{\partial t}(\rho_g h_g) + \frac{\partial}{\partial x}(\rho_g h_g U_g) = m_g \quad (5.36)$$

Using the above expressions for  $\alpha$  and  $\sigma$ , we have

$$\frac{\partial}{\partial t}(\rho_g \alpha h) + \frac{\partial}{\partial x}(\rho_g \alpha h \sigma U_e) = m_g \quad (5.37)$$

By means of the non-dimensional variables, this equation can be written

$$\frac{\partial}{\partial t^0}(\alpha \rho_g^0 h^0) + \frac{h_0 U_0}{Lf} \frac{\partial}{\partial x^0}(\rho_g^0 h^0 U_e^0 \alpha \sigma) = \frac{m_g}{f \rho_0}$$

Defining

$$\gamma = \left( \frac{h_0}{L} \right) \left( \frac{U_0}{f} \right)$$

we obtain

$$\frac{1}{\gamma} \frac{\partial}{\partial t^0}(\alpha \rho_g^0 h^0) + \frac{\partial}{\partial x^0}(\rho_g^0 h^0 U_e^0 \alpha \sigma) = \frac{1}{\gamma} \rho_g^0 \left( \frac{J(t)}{J} \right) \left( \frac{e_g}{e_a} \right) \left( \frac{\rho_a}{\rho_g} \right) \quad (5.38)$$

Now the quantities  $x^0, t^0, h^0, U_e^0, \alpha, \sigma, J(t)/J$  are all of unit order of magnitude. That is, all the terms in a non-dimensionalised kinematic equation must be retained.

The non-dimensional quantity  $\gamma$  can be regarded as the ratio of two time constants for the process,  $h_0/f$  and  $L/U_0$ . The former time constant is a measure of the time required for the cathode to travel a distance equal to the inlet electrode gap; the latter constant is a measure of the time for the electrolyte to travel through the electrode gap. If we insert typical values, we have

$$\frac{h_0}{f} \simeq [0(1)], \frac{L}{U_0} \simeq [0(10^{-3})]$$

i.e.

$$\gamma \simeq [0(10^3)].$$

Thus we conclude from Equation (5.38) that at the feed-rates used in ECM, the time-dependent changes in the mass flow occur instantaneously compared with the changes dependent upon position along the gap. In the same way, the transient terms in the other transport equations can be shown to be negligible.

These results mean that the void fraction, electrolyte temperature, and velocity reach local steady flow conditions almost instantaneously in response to transients associated with changes in the gap width given by the kinematic equation. It should be realised, however, that this analysis does not provide information about the time taken for the current density to reach an equilibrium value along the electrode length.

#### 5.4 Expression for the void fraction

We are now in a position to derive an expression for the void fraction,  $\alpha$ .

First, Equations (5.25) and (5.26) are integrated, the boundary conditions at  $x = 0$  being,

$$\alpha = 0, \quad h = h_0, \quad \rho_e = \rho_0, \quad U_e = U_0$$

The resulting equations can then be rearranged to give

$$hU_e = \frac{e_g Jx}{\rho_g \sigma \alpha}$$

and

$$hU_e = \frac{(e_a - e_g)Jx + \rho_0 h_0 U_0}{\rho_e (1 - \alpha)}$$

That is,

$$\frac{1 - \alpha}{\alpha} = \frac{[(e_a - e_g)Jx + \rho_0 h_0 U_0] \rho_g \sigma}{\rho_e e_g Jx} \quad (5.39)$$

If we use Equation (5.29)

$$\rho_e = \rho_0 \quad (5.29)$$

and, following Thorpe and Zerkle, we define

$$A = \frac{\rho_0 e_g}{\sigma \rho_g e_a} \quad (5.40)$$

then Equation (5.39) becomes

$$\frac{1 - \alpha}{\alpha} = \frac{(e_a - e_g)}{A e_a} + \frac{\rho_0 h_0 U_0}{A e_a Jx}$$

that is,

$$\alpha = \frac{A e_a Jx}{\rho_0 h_0 U_0 + A e_a Jx \left( 1 + \frac{e_a - e_g}{A e_a} \right)} \quad (5.41)$$

By introduction of the non-dimensional variables

$$e^* = \frac{e_a - e_g}{e_a} \quad \text{and} \quad x^* = \frac{x}{LS} \quad (5.42)$$

where

$$S = \frac{\rho_0 h_0 U_0}{L \rho_a f} \quad (5.43)$$

and which, on substitution for  $f$  from Equation (5.6), becomes

$$S = \frac{\rho_0 h_0 U_0}{L e_a J} \quad (5.44)$$

then Equation (5.41) takes the non-dimensional form

$$\alpha = \frac{Ax^*}{1 + (A + e^*)x^*} \quad (5.45)$$

Note that  $A$  depends inversely on the gas density  $\rho_g$  whose variation with distance  $x^*$  along the electrode has not been established. How-

ever, if the pressure drop across the gap is small,  $A$  can be assumed to be approximately constant.

## 5.5 Taper in width of equilibrium gap

### 5.5.1 Effects due to gas and heating

When Equation (5.26) is integrated, we obtain

$$\rho_e(1 - \alpha)hU_e = (e_a - e_g)Jx + \rho_0 h_0 U_0 \quad (5.46)$$

the constant of integration being evaluated from the boundary conditions

$$\rho_e h U_e = \rho_0 h_0 U_0$$

and

$$\alpha = 0$$

at

$$x = 0.$$

If the expression for  $(1 - \alpha)hU_e$  is substituted from Equation (5.46) into the energy equation (5.27), and if  $J$  is also eliminated from Equation (5.27) by use of Equation (5.6), Equation (5.27) becomes

$$\frac{dT}{dx^*} = \left( \frac{V}{e_a c_e} \right) \frac{1}{(1 + e^* x^*)} \quad (5.47)$$

Note that for simplicity the constant  $\Delta V$  has been neglected. The quantity  $V/e_a c_e$  can be regarded as a reference temperature,  $T_r$ . Equation (5.47) has the solution

$$T = T_0 + \frac{T_r}{e^*} \ln(1 + e^* x^*) \quad (5.48)$$

The variation in the equilibrium gap width due to hydrogen gas and heating can now be calculated. This analysis can be simplified, if it is assumed that the hydrogen bubbles completely fill the electrode gap. That is,

$$\delta_g = h$$

If overpotentials are also ignored, Equation (5.33) then reduces to

$$V = \frac{Jh}{\kappa_m}$$

At entry to the gap,

$$V = \frac{Jh_0}{\kappa_0}$$

By expressing  $\kappa_m$  in terms of  $\kappa_0$  from Equations (5.31) and (5.34), we can then deduce the local gap width:

$$\frac{h}{h_0} = (1 - \alpha)^n [1 + \xi(T - T_0)] \quad (5.49)$$

From Equations (5.45) and (5.48), the ratio  $h/h_0$  can be expressed in terms of the non-dimensional distance  $x^*$ :

$$\frac{h}{h_0} = \left[ \frac{1 + e^* x^*}{1 + (A + e^*) x^*} \right]^n \left[ 1 + \frac{B}{e^*} \ln(1 + e^* x^*) \right] \quad (5.50)$$

where  $B = \xi T_r$

Let us now compare the variations in gap width due to heating and hydrogen gas separately.

### 5.5.2 Effects due to heating

If the presence of hydrogen gas is ignored, we may put  $\alpha = 0$  in Equation (5.49), and substitution for  $(T - T_0)$  from Equation (5.48) gives

$$\frac{h}{h_0} = \left[ 1 + \frac{\xi T_r}{e^*} \ln(1 + e^* x^*) \right] \quad (5.51)$$

### 5.5.3 Effects due to hydrogen gas

This variation can be obtained in a similar fashion to that of the above section; ignoring electrolyte heating, we have

$$\begin{aligned} \frac{h}{h_0} &= (1 - a)^n \\ &= \left[ \frac{1 + e^* x^*}{1 + (A + e^*) x^*} \right]^n \end{aligned} \quad (5.52)$$

Expressions (5.45), (5.51), and (5.52) can be simplified further by approximations for  $e^*$  and  $e^*x^*$  which are based on practical values for the process variables.

Consider Equation (5.42):

$$x^* = \frac{\rho_a f x}{\rho_0 U_0 h_0}$$

For the values  $\rho_a = 8 \text{ g/cm}^3$ ,  $\rho_0 \approx 1 \text{ g/cm}^3$ ,  $h_0 = 0.4 \text{ mm}$ ,  $U_0 = 1.5 \text{ m/s}$ ,  $f = 1.66 \times 10^{-2} \text{ mm/s}$ ,  $e_a = 29 \times 10^{-5} \text{ g/C}$ ,  $e_g = 1 \times 10^{-5} \text{ g/C}$ ,  $x^* \approx 2 \times 10^{-3}$  to  $2 \times 10^{-2}$  for  $x$  ranging from 10 to 100 mm. Also  $e^* < 1$ , so that  $e^*x^* \ll 1$ .

For this condition for  $e^*x^*$ , approximations to the solutions (5.45), (5.51), and (5.50) can be deduced:

$$\alpha = \frac{Ax^*}{1 + Ax^*} \quad (5.53)$$

$$\frac{h}{h_0} = (1 + \xi T_r x^*) \quad (5.54)$$

$$\frac{h}{h_0} = \frac{1 + Bx^*}{(1 + Ax^*)^n} \quad (5.55)$$

From Equation (5.54) note that, with Joule heating only, the gap increases linearly with distance along the electrode. This result is the same as that obtained by Tipton [15] who implicitly used both the energy equation and the approximation that  $e^*x^* \ll 1$ .

These equations demonstrate the significance of the quantities  $A$  and  $B$ . From Equation (5.53),  $A$  represents the effect of the void fraction, whilst from Equation (5.54),  $B$  is a measure of the effect of heating. In Equation (5.55), if  $n = 1$  and  $A = B$ , the effect of the hydrogen gas is balanced by the temperature effect.

#### 5.5.4 Effect due to polarisation

One other effect on the gap width needs consideration. The presence of overpotentials at the electrodes can have the apparent effect of increasing the gap width between the electrodes. This phenomenon is well known in electrodeposition, and in Chapters 6 and 7 an analysis is carried out to establish the characteristic, corresponding behaviour in ECM. Although that analysis demonstrates mainly the effect of overpotentials on the processes of anodic smoothing and

shaping, it also shows that the width of the gap is increased by an apparent amount

$$\kappa_e \frac{\partial f(J)}{\partial J}$$

which quantity is evaluated for values of a defined mean current density. Here  $f(J)$  is a current density-dependent overpotential at the cathode.

#### Example

Suppose that the Tafel equation applies at the cathode  $\eta_a = a + b \log J$ . The apparent increase in gap width due to that overpotential alone is  $\kappa_e b/J$ . For typical values,  $\kappa_e = 0.1 \text{ ohm}^{-1} \text{ cm}^{-1}$ ,  $b (= 2.3 RT/z\alpha F)$ , where  $\alpha \approx 0.5$ ,  $z = 1$ ,  $RT/F = 1/40 \text{ V}$ ,  $J = 50 \text{ A/cm}^2$ , the apparent increase in gap is about  $2.3 \times 10^{-3} \text{ mm}$ . This calculation indicates that the overpotential has little effect in increasing the gap, which, typically, is about 0.4 mm.

#### 5.5.5 Further studies of gap variation

In Fig. 5.13 the theoretical expression (5.55) for the variation in gap width with distance along the electrode length is compared with the experimental results obtained by Hopfenfeld and Cole. Both investigations show that the gap becomes convergent in the downstream direction.

Nevertheless, some comments must be made on these results. The theoretical curve was derived on the assumption that the quantity  $A$  is constant. This assumption is a reasonable one, provided that the pressure drop along the gap is small. This was the case for the experimental work discussed in relation to Fig. 5.13.

However, at higher pressure drops or lower flow-rates, a constant value for  $A$  cannot be assumed, and the simple theory breaks down. (Experimental results for higher pressures are described below.)

The index  $n = 1.5$  has been used on the basis of a uniform distribution of gas bubbles across the gap. That is,  $\delta_g = h$ . As has been seen in Section 5.2, however, an accumulation of bubbles close to the cathode surface appears to be more likely. Since a greater reduction of current should then occur, a value of  $n$  greater than 1.5 would seem more acceptable. Accordingly, a further curve, for  $n = 2$ , has also been produced, and, as shown in Fig. 5.13, closer agreement with the experimental results is obtained.

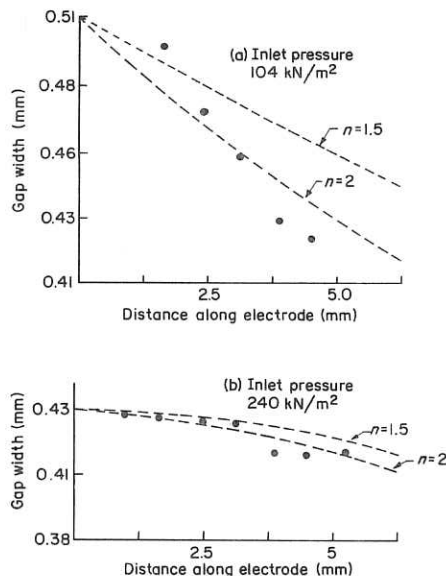


Fig. 5.13 Variation in gap width with distance along the electrode; 0.67N KCl electrolyte; rectangular Al anodes 6.35 mm x 9.53 mm;  $T_0 = 24^\circ\text{C}$  (a),  $27^\circ\text{C}$  (b);  $V = 19.5$  V (a), 19 V (b);  $Q_0 = 1.4 \times 10^{-8} \text{ m}^3/\text{s}$  (a),  $6.5 \times 10^{-8} \text{ m}^3/\text{s}$  (b);  $I \approx 19$  A (a), 28 A (b) (after Thorpe and Zerkle [10])

Higher pressure drops, from 14 MN/m<sup>2</sup> at gap inlet to 69 kN/m<sup>2</sup> at outlet, with correspondingly high electrolyte velocities, have been used in further investigations of the variation in gap shape [16, 17]. The variation in gap found for these conditions is shown in Fig. 5.14. [In that figure both coordinates are plotted in dimensionless form, the suffix 0 denoting the inlet condition. When the gap ratio,  $h(x)/h_0 - 1$ , is zero there is no taper of the gap, when the ratio is positive the gap is divergent, and when it is negative the gap is convergent.]

The figure shows that the taper is divergent. That is, electrical heating has predominated over hydrogen gas in affecting the effective conductivity of the electrolyte solution, and hence the shape of the gap. The result is attributed to the high electrolyte flow-rates and pressures, which considerably reduce the specific volume of hydrogen gas bubbles. That reduction then permits a greater influence of electrical heating on the effective conductivity of the electrolyte.

These variations in shape of the gap which have been discussed suggest that further investigations of the effects of gas generation and electrical heating are necessary. Much information can stem

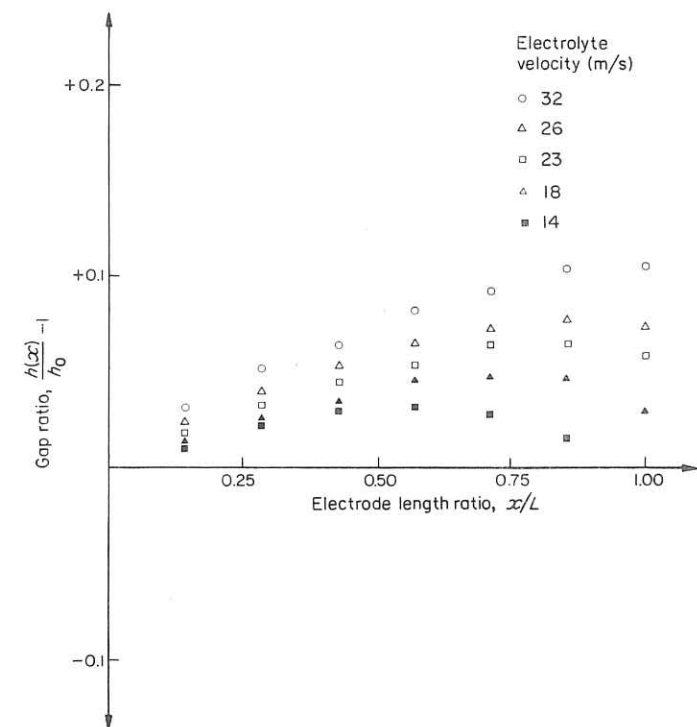


Fig. 5.14 Variation in gap width with electrolyte velocity; 2.5N NaCl; 0.038 m x 0.076 m rectangular electrodes; mild steel anode;  $V = 20$  V;  $J = 48$  A/cm<sup>2</sup>;  $f = 16.7 \times 10^{-3}$  m/s;  $h_0 = 0.5$  mm; pressure = 14 MN/m<sup>2</sup> (inlet), 69 kN/m<sup>2</sup> (outlet) (after Clark, McGeough and Yeo [16])

from studies of the velocity, pressure, and temperature distribution of the flowing electrolyte solution during ECM.

## 5.6 Velocity distribution along electrode length

The evolution of hydrogen and electrical heating also cause a variation in the velocity distribution along the electrode. Thorpe and Zerkle have obtained an analytic expression for this variation, although they do not consider any variation in the regions of the

boundary layers. Using Equations (5.26), (5.45), and (5.50), they derive

$$\frac{U_e}{U_0} = \frac{[1 + (e^* + A)x^*]^{n+1}}{(1 + e^*x^*)^n \left[ 1 + \frac{B}{e^*} \ln(1 + e^*x^*) \right]} \quad (5.56)$$

The authors point out that if the pressure drop is small compared to ambient pressure, the quantity  $A$ , which is really a function of position, will be essentially constant. The equation can be reduced further if, as is usually the case, the coordinate  $x^*$  is of order of  $10^{-2}$  or less; since  $e^* < 1$ , then  $e^*x^* \ll 1$ . The above equation becomes

$$\frac{U_e}{U_0} = \frac{(1 + Ax^*)^{n+1}}{1 + Bx^*} \quad (5.57)$$

### 5.7 Pressure distribution along electrode length

In Chapter 2 expressions were derived for the pressure drop along a rectangular channel for single-phase flow (Sections 2.6 and 2.9). The basis of that work was that established hydrodynamic theory was applicable to (particularly) turbulent flow down small channels of dimensions similar to those met in ECM. In fact, little is known of the hydrodynamic phenomena which may arise under these geometric conditions.

Hopenfeld and Cole<sup>7</sup> have carried out some single-phase flow experiments on the variation of the friction factor with distance along a rectangular channel, of breadth and gap width 9.5 mm and 0.375 mm respectively, for Reynolds numbers ranging from 4500 to 15 000. Their main results show that, as the Reynolds number is increased, the friction factor decreases, and that for values of the ratio, distance along the electrode to hydraulic diameter, greater than 50, the friction factor coincides with that obtained from the Blasius relation for fully developed turbulent flow. It is emphasised, however, that these experiments were carried out without ECM.

Further information is available in other studies which have indicated that the conventional relationships between Nusselt number and Reynolds number and Schmidt number are applicable to ECM conditions [18]. On that basis, the conventional formulae for pressure drop and diffusion layer thicknesses for linear flow between closely spaced electrodes have been used in the determina-

tion of the data in Table 5.2. It is pointed out that these thin layer thicknesses and high rates of transport mean that very high power is required to pump the electrolyte through such small gaps.

Table 5.2 Pressure drop and diffusion layer thickness for linear flow of electrolyte between electrodes of gap 0.5 mm;  $\rho_e = 1 \text{ g/cm}^3$ ,  $\nu = 1 \text{ mm}^2/\text{s}$ ,  $D = 4 \times 10^{-6} \text{ cm}^2/\text{s}$   
(after Tobias [18])

Reynolds number	Velocity (m/s)	Pressure drop (atm/cm)	Diffusion layer (mm)
10 000	10	$1.5 \times 10^{-1}$	$2.0 \times 10^{-3}$
20 000	20	$4.9 \times 10^{-1}$	$1.1 \times 10^{-3}$
100 000	100	8.2	$3.2 \times 10^{-5}$

In ECM, moreover, the presence in the electrolyte solution of the products of the reactions at both electrodes means that the flow patterns should differ from those of a single-phase flow. Attention has already been drawn in Chapter 2 to one change that arises with these multi-phase flow conditions: a higher inlet pressure is now required to maintain the same rate of flow of electrolyte solution.

### 5.8 Temperature distribution along electrode length

In the course of the analysis in Section 5.5, an expression was derived for the temperature rise along the electrode length:

$$T(x^*) = T_0 + \frac{T_f}{e^*} \ln(1 + e^*x^*) \quad (5.48)$$

For the usual approximation,  $e^*x^* \ll 1$ , and on substitution of the process variables, Equation (5.48) reduces to

$$T(x) - T_0 = \frac{VJx}{c_e \rho_e h_0 U_0}$$

where Equation (5.6) has also been used. That is, a linear increase in temperature with distance along the gap should be expected. The assumptions, previously discussed, including low pressure drop along the electrode length, still hold.

The problem of electrical heating of the electrolyte has received much attention, often in relation to the limitations imposed on the

process by excessive heating, or boiling. It will be recalled that, in Chapter 1, estimates of the Joule heating of the solution provided a simple means of estimating typical electrolyte velocities in ECM.

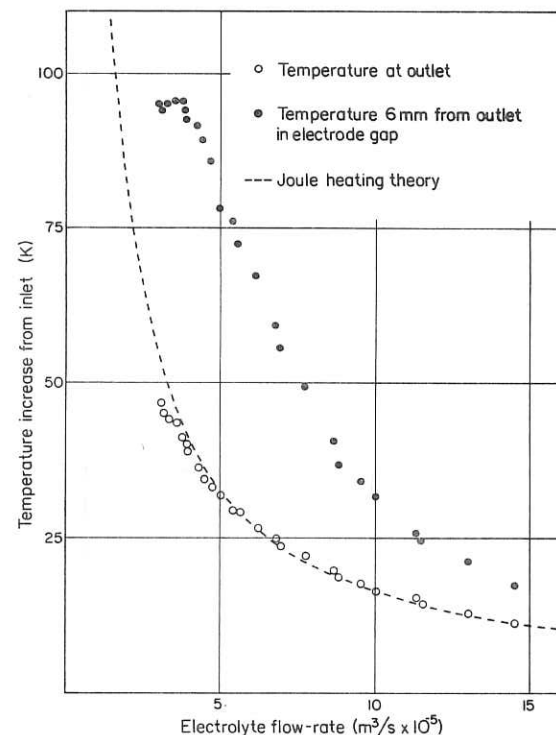


Fig. 5.15 Variation in temperature increase with electrolyte flow-rate;  
 $J = 16 \text{ A/cm}^2$ ;  $V = 32 \text{ V}$ ; pressure =  $170 \text{ KN/m}^2$  (outlet);  $f = 6 \times 10^{-3} \text{ mm/s}$   
(after Clark and McGeough [19])

Results of measurement of the temperature variation of a 10% (w/w) NaCl solution, flowing down a rectangular channel of length, breadth, and inlet width 100 mm, 13 mm, and 2.4 mm, respectively, are shown in Fig. 5.15. In this work, the inlet temperature was  $20^\circ\text{C}$  and little pressure drop occurred between inlet and outlet.

The electrolyte temperature rise, measured at inlet and outlet points, shows good agreement with the increase calculated from ohmic resistance heating theory [Equation (5.48)]. However, the temperatures measured within the electrode gap, just before outlet (6 mm), are seen to be greater than those at outlet. As the flow-rate

is reduced, the temperature within the gap increases to a maximum value which corresponds closely to the boiling state of the electrolyte. Fluctuations in the machining current and voltage were observed for this condition, and the more the flow-rate was reduced, the further upstream occurred the point of onset of the boiling condition.

The higher temperatures within the gap are consistent with measurements carried out in a region of increased resistivity. Such local conditions would be provided by a hydrogen bubble-electrolyte mixture adjacent to the cathode in which the temperature of the electrolyte around the bubbles would be higher than that in the bulk of the solution.

On the assumption that this boiling condition in the gap is largely induced by the presence of hydrogen gas, the use of an electrolyte like sodium nitrate should provide some striking differences in behaviour

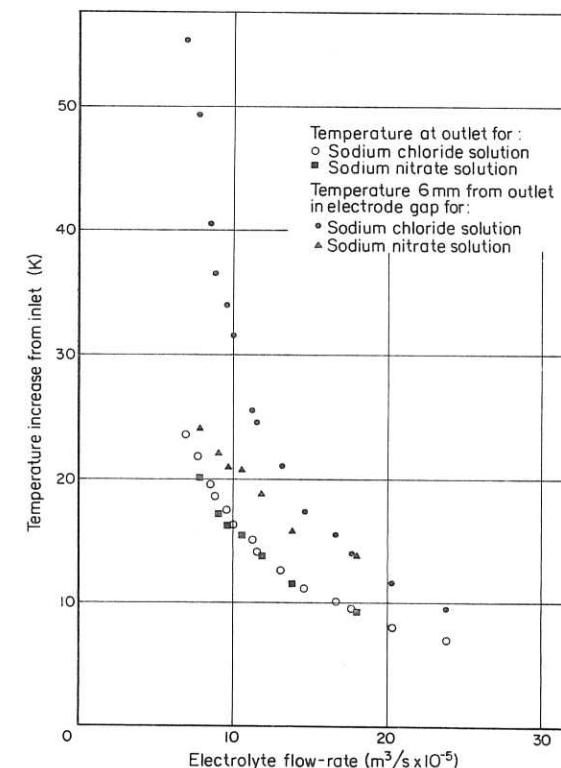


Fig. 5.16 Temperature increase for sodium chloride and sodium nitrate electrolytes (after Clark and McGeough [19])

from those of NaCl solution. It will be recalled from Chapter 4 that mild steel is machined with substantially less hydrogen gas evolution in nitrate electrolytes. Indeed, tests carried out with a 17% (w/w) NaNO<sub>3</sub> solution under the same operating conditions did yield quite contrasting results. [A 17% (w/w) NaNO<sub>3</sub> solution has the same conductivity as a 10% (w/w) NaCl solution.] In Fig. 5.16, temperatures measured at outlet are comparable with those obtained for the tests with the chloride solution. At high flow-rates, temperatures within the gap are also similar to those in the NaCl test series. At lower flow-rates, however, these temperatures within the gap are lower than those for the equivalent chloride tests. With this reduction in flow-rate there was an associated decrease in current efficiency, from almost 70% to small values (about 2 to 5%), corresponding to conditions of virtually complete passivation, at the highest and lowest flow-rates respectively. (Current efficiencies were based on divalent metal removal.) At virtual passivation conditions, the temperature within the gap is only slightly greater than that at outlet. This observation may be related to the work of Mao who found that no hydrogen was evolved at the cathode under conditions of low current efficiency when machining mild steel with nitrate solutions (see Chapter 4). Three distinct trends in variation of gap width were also determined from these experiments. For current efficiencies close to 70%, the electrode gap increased slightly along the electrode length. As the current efficiency decreased with flow-rate, the gap became gradually convergent; whilst for conditions of virtually complete passivation the gap remained constant along the electrode length.

These experiments also bring to light two conditions which can limit the rate of machining: boiling of the electrolyte and passivation. These conditions, and others which impose limitations on the rate of ECM, are discussed in the next section.

## 5.9 Limitations on the rate of electrochemical machining

### 5.9.1 Electrolyte boiling

In Chapter 1, a simple calculation was carried out to estimate the electrolyte flow-rate required to prevent the electrolyte boiling at the gap exit. The study of boiling phenomena in the section above demonstrated that boiling must be prevented throughout the length

of the gap, as well as at outlet. A further restraint, accordingly, has to be imposed on any analysis which defines the conditions for the prevention of boiling. In terms of the theory of temperature distribution in the previous section, even a simple condition for no boiling would now become

$$(T_b - T_0) > \left( \frac{V}{e_a c_e} \right) \left( \frac{x}{h_0} \right) \left( \frac{\rho_a}{\rho_0} \right) \left( \frac{f}{U_0} \right)$$

where  $x$  is now evaluated at some point along the electrode length at which the electrolyte first boils at temperature  $T_b$ . The above condition still indicates, though, that if the velocity,  $U_0$ , is increased, boiling will occur further downstream, and that the boiling state will be advanced if the applied voltage and feed-rate are increased.

From Section 5.8, it is again noted that, with the onset of boiling, violent fluctuations in the cell current and voltage are likely to arise.

### 5.9.2 Sparking

The rate of machining can also be limited by sparking; with its onset, machining is usually terminated. A further effect is often electrode wear. (In practice, possible damage to the cathode can be diminished by the use of materials like stainless steel and tungsten alloys.) Sparking and electrical breakdown in ECM appear to be associated with the formation of a gas blanket over one of the electrodes. Its occurrence is also greatly influenced by the electrolyte velocity; if the flow-rate is sufficiently high, sparking is usually prevented. However, if the flow-rate is reduced, large voltage fluctuations, and eventually sparking, occur. Related oscillations in the cathode potential and cell voltage usually indicate that the phenomena are cathodic in origin [5, 8]. It has also been claimed that their onset coincides with the appearance of a different type of gas bubble, which is large and irregular in shape. This type of formation replaces the more frequent, small individual gas bubbles. The new continuous gas pocket may also cover a large part of the cathode surface, and even if it only instantaneously covers the complete surface, sparking results. The volume fraction at which sparking occurs has been estimated to be about 0.2 at 100 and 150 A/cm<sup>2</sup>, the flow-rate being 5 to 10 m/s (equivalent to 20 to 40 × 10<sup>-6</sup> m<sup>3</sup>/s).

If, owing to the presence of non-conducting gas bubbles, the gap develops a sufficiently steep taper, direct physical contact, and sparking, may ensue between anode and cathode. The tapering of

the gap was discussed in Section 5.5. It was seen then that this problem can be diminished by use of higher flow-rates.

### 5.9.3 Cavitation

The presence of cavitation bubbles within the machining gap may also cause machining to be terminated, since these bubbles form non-conducting regions. Moreover, cavitation has been a suggested cause of some very rough, striated finishes in ECM. Clearly, surface roughness of sufficient magnitude can also lead to direct contact between anode and cathode causing an electrical short-circuit.

The simplest means of overcoming cavitation is by the application of an outlet pressure. This procedure has been discussed in Section 2.10.3.

Limitations on the electrode feed-rate due to cavitation have been the subject of a detailed theoretical study of electrolyte flow between shallow, axially symmetric cavities [11]. For a flat-bottomed cathode and for flow in the outward direction, an analysis of the transport equation for momentum, with use of typical numerical values has yielded the set of curves given in Fig. 5.17. Each curve was computed for an absolute pressure at inlet to the machining gap, in a range from about 0.06 times to twice atmospheric pressure. The absolute pressure at outlet to the gap was also about twice atmospheric, and the inlet temperature was 38°C. Since the saturation pressure corresponding to this temperature is approximately 0.06 times atmospheric value, curve (a) indicates a cavitation limit. That is, cavitation would occur at the gap inlet for feed-rate/flow-rate com-

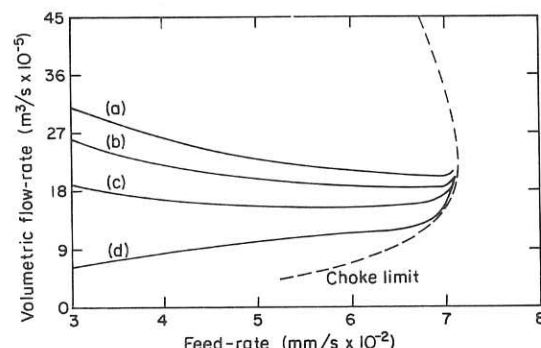


Fig. 5.17 Cavitation limitations on feed-rate. Absolute pressure (atm.) at gap inlet: (a) 0.068, (b) 0.68, (c) 1.36, (d) 2.04 (after Thorpe and Zerkle [11])

bination which lie above the curve (a) limit. ECM is also impossible beyond the broken line on the right of Fig. 5.17. This limitation is imposed by choking. It is discussed more fully below, in relation to flow down a rectangular channel.

### 5.9.4 Choking

In Chapter 2, the basic principles of choking were outlined. This phenomenon is often encountered in compressible fluid flow or in two-phase fluid flow without ECM. The presence of compressible hydrogen gas in ECM flow means that choking is another possible limitation on the rate of machining. Although no reports are yet available of choking observed in ECM, a theoretical analysis provides some insight into the limiting physical conditions which are imposed by the onset of choking [10].

Because this analysis is rather lengthy, only its main points are summarised here. Essentially, the analysis consists of an examination of the transport equation of motion for flow along a rectilinear gap in ECM. By use of the assumed equation of state, (5.28), a differential equation is obtained for the variation along the electrode length of the hydrogen gas density:

$$\frac{dA}{dx^*} = \frac{\frac{CT_r^0 Z^3}{2A} - BY^{2n+1} + A(n+1)Y^{2n}Z + \left(\frac{SMK_0}{4}\right)Y^{3n+2}}{\frac{C(1+T_r^0 x^*)Z^3}{2A^2} - (n+1)Y^{2n}Zx^*} \quad (5.58)$$

Here the gas density is expressed in terms of the function,

$$A = \frac{\rho_0 e_g}{\sigma \rho_g e_a} \quad (5.40)$$

In addition,

$$x^* = \left(\frac{x}{h_0}\right) \left(\frac{\rho_a}{\rho_0}\right) \left(\frac{f}{U_0}\right) \quad (5.42)$$

$$C = \frac{2}{\sigma} \left(\frac{e_g}{e_a}\right) \left(\frac{RT_0}{U_0^2}\right)$$

$$T_r = \frac{V}{e_a c_e}$$

$$Z = (1 + Bx^*)$$

$$Y = (1 + Ax^*)$$

where  $B = \xi T_r$ .

Here  $M$  is the frictional pressure drop multiplier for two-phase flow.  $K_0$  is the pressure loss coefficient for a rectilinear gap without ECM.

We recollect that the superscript 0 denotes a dimensionless quantity, and that

$$S = \frac{\rho_0 h_0 U_0}{\rho_a L f}$$

The important point about Equation (5.58) is the possibility of a singularity. That is, as  $x^*$  increases from zero value at the gap inlet, the denominator will eventually become zero. This condition corresponds to 'choking'. It will become clear below that the choking condition at the gap exit corresponds to a limiting value of the cathode feed-rate. If choking is to be avoided, the denominator must not become zero for any position along the gap. In particular, at the gap exit, where  $x^* = 1/S$ , we must have

$$\frac{C \left(1 + T_r^0 \frac{1}{S}\right) \left(1 + B \frac{1}{S}\right)^2}{2A_e^2} > \frac{(n+1) \left(1 + A_e \frac{1}{S}\right)^{2n}}{S} \quad (5.59)$$

It can also be shown that, at the gap exit,

$$A_e = \frac{C}{p_e^0} \left(1 + T_r^0 \frac{1}{S}\right) \quad (5.60)$$

Here the subscript e denotes the exit condition. When Equation (5.60) is substituted into Equation (5.59), the following expression is obtained

$$\frac{2(n+1)C(S + T_r^0)[S^2 p_e^0 + C(S + T_r^0)]^{2n}}{(S + B)^2 p_e^{0(2(n+1))} S^{4n}} < 1 \quad (5.61)$$

If all process variables, except gap width  $h_0$ , electrolyte velocity at inlet  $U_0$ , electrolyte pressure  $p_e$ , and index  $n$  are known, then the constants  $C$ ,  $T_r^0$ , and  $B$  can be computed. Since  $S$  is proportional to  $U_0 h_0^2$ , and  $p_e^0$  to  $p_e/U_0^2$ , Equation (5.61) can be evaluated for different combinations of the quantities  $h_0$ ,  $U_0$ ,  $p_e$ , and  $n$ . Thorpe and Zerkle show that, if choking is to be avoided, only a limited range of inlet velocities  $U_0$  is available for each  $h_0$ ,  $p_e$ , and  $n$ . Some of their results are shown in Fig. 5.18. For outlet pressures of 101 and 102 kN/m<sup>2</sup> and  $n$  values of 1, 1.5, and 2, acceptable values of

the gap width at inlet,  $h_0$ , are to the right of each curve shown. Since the feed-rate  $f$  is inversely proportional to  $h_0$ , the exit pressure and  $n$  have a significant influence on the maximum feed-rate.

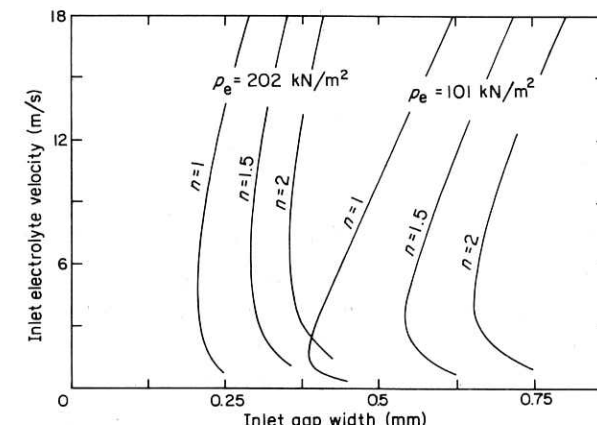


Fig. 5.18 Limitations imposed by choking on inlet flow velocity,  $U_0$ , and inlet gap width,  $h_0$ ;  $\kappa_0 = 0.2 \text{ ohm}^{-1} \text{ cm}^{-1}$ ;  $L = 25.4 \text{ mm}$ ;  $T_0 = 20^\circ\text{C}$ ,  $e_a = 29 \times 10^{-5} \text{ g/C}$ ;  $e_g = 10^{-5} \text{ g/C}$ ;  $v = 1 \text{ mm}^2/\text{s}$ ;  $\sigma = 1$ ;  $\rho_a = 7.8 \text{ g/cm}^3$ ;  $\rho_0 = 1 \text{ g/cm}^3$  (after Thorpe and Zerkle [10])

### 5.9.5 Passivation

In the course of Chapter 4 many examples were given of the limitations on the rate of ECM arising from a passivating film on the anode surface. Even in Section 5.8, passivation was shown to impose considerable restrictions on the machining of mild steel in sodium nitrate solution. From that study, one other result is of interest: a computation of the Nusselt number for the passivation conditions [17]. (The basis of this calculation is also outlined in Chapter 4.)

The Nusselt number is

$$Nu = \frac{J_l d_h}{z F C_b D}$$

where  $J_l$  is the limiting current density,  $d_h$  the hydraulic mean diameter,  $z$  the valency of the dissolving metal ions,  $F$  the Faraday,  $C_b$  the bulk concentration of the reacting species, and  $D$  the diffusion coefficient.

Suppose that  $J_1$  is determined from the experimentally observed current density at passivation ( $16 \text{ A/cm}^2$ ), and  $C_b$  is replaced by a possible saturation concentration value (say, 5 mole/litre). On substitution of these values together with  $d_h = 4 \text{ mm}$ ,  $z = 2$ ,  $F = 96\,500 \text{ C}$ ,  $D = 1.5 \times 10^{-5} \text{ cm}^2/\text{s}$ , the Nusselt number is calculated to be about 440.

Although this estimate indicates the order of magnitude of the Nusselt number, the value of the number would clearly be changed on the substitution of some other possible saturation concentration.

#### 5.9.6 Limiting current densities for ionic mass transport

The maintenance of the electrode reactions in ECM requires that the anodic and cathodic products be removed from the neighbourhood of the electrodes and that reactants be introduced. The movement of the dissolved particles has been shown in Chapter 3 to be describable in terms of the Nusselt number, with which are usually associated the Reynolds and Schmidt numbers (Equations (3.32) to (3.38)).

Landolt et al. [20] suggest that these relationships can be used to predict limiting current densities in ECM. They point out that, since the anodic dissolution products have to be removed from the anode region, the dissolution rate may be checked by the limit of solubility of the reaction products. They advocate, therefore, that the  $C_b$  term in these expressions be replaced by a term,  $\Delta C$ , for the concentration difference between the interface and the bulk solution which is a measure of the solubility. For example,  $\Delta C = 0.1$  to 10 mole/litre could represent concentration differences ranging from weakly to well soluble conditions. Clearly, the limiting current densities in conditions for which  $\Delta C = 10 \text{ mole/litre}$  will be higher than those for which  $\Delta C = 0.1 \text{ mole/litre}$ .

#### References

1. McGeough, J. A. and Rasmussen, H., *Trans. A.S.M.E. Series B, J. Eng. Ind.* (1970) No. 2, 400.
2. Johnson, M. P. and Brown, D. J., Dept. Trade & Ind. Report, Contract No. KJ/4M/117/CB78A (1970) July.
3. Ito, S., Chikamori, K. and Hayashi, T., *J. Mech. Lab. Japan* (1964) 10, No. 2, 33.
4. Noble, C. F. and Shine, S. J., Paper presented at First Int. Conf. on ECM, Leicester University, Mar. 1973.
5. Landolt, D., Acosta, R., Muller, R. H. and Tobias, C. W., *J. Electrochem. Soc.* (1970) 117, No. 6, 839.
6. Hopenfeld, J. and Cole, R. R., *Trans. A.S.M.E., J. Eng. Ind.* (1966) 88, No. 4, 455.
7. Hopenfeld, J. and Cole, R. R., *Trans. A.S.M.E., J. Eng. Ind.* (1969) Aug., No. 8, 755.
8. Baxter, A. C., Ph.D. Thesis, University of Warwick (1967).
9. Baxter, A. C., Freer, H. E. and Willenbruch, D. A., Paper presented at First Int. Conf. on ECM, Leicester Univ., Mar. 1973.
10. Thorpe, J. F. and Zerkle, R. D., *Int. J. Mach. Tool Des. Res.* (1969) 9, 131.
11. Thorpe, J. F. and Zerkle, R. D., in *Fundamentals of ECM* (ed. C. L. Faust), see Ref. 8, Ch. 4, 1.
12. Thorpe, J. F., Paper presented at Soc. Manuf. Eng. Conf., Detroit, 1970, Paper No. MR-70-513.
13. Bass, L., *Trans. Faraday Soc.* (1964) 60, 1646.
14. De la Rue, R. E. and Tobias, C. W., *J. Electrochem. Soc.* (1959) Sept, 827.
15. Tipton, H., Proc. Fifth Int. Conf. Mach. Tool Res., Birmingham (1964) Sept., p. 509.
16. Clark, W. G., McGeough, J. A. and Yeo, J. T., unpublished work.
17. Clark, W. G., Ph.D. Thesis, Strathclyde University, Glasgow (to be submitted).
18. Tobias, C. W., Paper presented at First Int. Conf. on ECM, Leicester University, Mar. 1973.
19. Clark, W. G. and McGeough, J. A., Paper presented at First Int. Conf. on ECM, Leicester University, Mar. 1973.
20. Landolt, D., Muller, R. H. and Tobias, C. W., in *Fundamentals of ECM* (ed. C. L. Faust), see Ref. 8, Ch. 4, p. 200.